Journal of Electrocardiology 97 (2026) 154272

Contents lists available at ScienceDirect

Journal of Electrocardiology

journal homepage: www.jecgonline.com

Evaluation of new vectorcardiography algorithms for identifying left ventricular hypertrophy and impaired systolic function

Janek Salatzki [a,b,*], Arne Kristian Schwarz [c,d], Sarah Wolfsteller [a], Nicolas Hein [a], Erika Poyo Medina [a], Norbert Frey [a], Henning Steen [a], Florian André [a], Alexander Passow [d,e]

[a] Department of Cardiology, Angiology and Pneumology, Heidelberg University Hospital, 69120 Heidelberg, Germany
[b] William Harvey Research Institute, NIHR Barts Biomedical Research Centre, Queen Mary University of London, Charterhouse Square, London EC1M 6BQ, UK
[c] Marienkrankenhaus Hamburg, Centre for Cardiovascular Imaging, Hamburg, Germany
[d] Cardisio GmbH, Frankfurt, Germany
[e] Universität Leipzig, Medizinische Fakultät, Institut für Medizinische Informatik, Statistik und Epidemiologie (IMISE), Leipzig, Germany

ARTICLE INFO

Keywords:
Vectorcardiography
Artificial intelligence
Impaired systolic function
Left ventricular ejection fraction
Left ventricular hypertrophy
Screening

ABSTRACT

Background: Timely diagnosis of impaired systolic function and left ventricular hypertrophy (LVH) remains a clinical challenge. Routine electrocardiography provides limited diagnostic accuracy for detecting early or subtle structural abnormalities. Vectorcardiography (VCG), which captures the spatial and temporal characteristics of cardiac electrical activation and repolarization, may offer a rapid, scalable, and cost-effective alternative for screening structural heart disease.
Objective: To evaluate the diagnostic performance of VCG for identifying impaired systolic function and left ventricular hypertrophy compared with cardiac magnetic resonance imaging.
Methods: This prospective case-control study included 245 participants undergoing both CMR and VCG. Among 245 participants, 40 had reduced LVEF (<40%) and 208 met CMR criteria for LVH; 34 patients had both conditions. Patients were classified as having impaired systolic function (left ventricular ejection fraction [LVEF] <40%), LVH (indexed left ventricular mass $\geq$ 55 g/m^2), or controls with structurally normal hearts. VCG was obtained using a five-lead system (cardisiography), and signals were processed by an AI algorithm extracting 583 parameters. Diagnostic performance was evaluated using CMR as reference.
Results: The repolarization time-difference ratio (Rpeak–Tonset / QRSend–Tpeak) showed the best diagnostic performance for impaired systolic function, with an area under the curve (AUC) of 0.843, sensitivity of 80.0%, and specificity of 83.9%. In LVH patients, three parameters—T-wave azimuth, T-wave magnitude, and azimuth variability—showed AUCs ranging from 0.739 to 0.791. Overall diagnostic accuracy was 81.7% for impaired systolic function and 78.2% for LVH, and 83.1% for the combined phenotype of reduced LVEF and LVH.
Conclusion: VCG reliably detects left ventricular systolic dysfunction and hypertrophy. This approach offers a scalable and interpretable screening tool, especially valuable in settings with limited access to advanced cardiac imaging. Future multicenter studies are needed to validate these findings and support clinical implementation.

Introduction

Heart failure (HF) with reduced ejection fraction is a significant public health concern, with rising prevalence and persistently high rates of mortality and morbidity (1,2). Left ventricular hypertrophy (LVH) is prognostically relevant for HF and other cardiovascular diseases (3,4). Early diagnosis of both HF and LVH is crucial for initiating timely treatment. However, these cardiac alterations present diagnostic challenges due to their often subtle and gradual progression (5). Non-invasive techniques play a critical role in early detection, allowing for more effective treatment. Echocardiography is recommended for both the initial evaluation and ongoing follow-up of patients with heart

Abbreviations: AUC, area under the curve; BMI, body mass index; CAD, coronary artery disease; CMR, cardiac magnetic resonance; CSG, cardisiography; ECG, electrocardiography; EF, ejection fraction; LGE, late gadolinium enhancement; LV-EF, left ventricular ejection fraction; LVH, left ventricular hypertrophy; VCG, vectorcardiography.

* Corresponding author at: Department of Cardiology, Angiology and Pneumology, Heidelberg University Hospital, 69120 Heidelberg, Germany.
E-mail address: janek.salatzki@med.uni-heidelberg.de (J. Salatzki).

https://doi.org/10.1016/j.jelectrocard.2026.154272

Available online 2 May 2026

failure or cardiomyopathy (6,7). Additionally, cardiac magnetic resonance imaging (CMR) is advised for the initial assessment of patients with cardiomyopathy (7). However, both echocardiography and CMR are resource-intensive, often associated with high costs, long waiting times, and the need for specialized personnel. Consequently, there is a growing demand for a faster, cost-effective, and easily accessible non-invasive testing method to detect functional and structural alterations.

Electrocardiography (ECG) is a key component of patient's initial evaluation and follow-up (8,9). However, traditional ECG methods have limited sensitivity in detecting these conditions due to their two-dimensional nature (8,9). In contrast, vectorcardiography (VCG) offers richer spatial and temporal information than the 2D surface ECG. Modern clinical VCG traces back to mid-20th-century developments (e.g., Frank's orthogonal lead system), followed by periods of waning clinical use and later revival through mathematical synthesis of VCG from standard 12-lead ECG and, most recently, AI-assisted analysis (10–12). These advances enable robust assessment of depolarization–repolarization vectors with established diagnostic and prognostic value. It enables a spatial representation of the entire electrical conduction process in one plane, in contrast to an ECG. By recording signals in three planes (horizontal, frontal, and sagittal), a spatial representation is achieved (12–14). This might offer new diagnostic possibilities in detecting HF and LVH.

The aim of this study is to evaluate the diagnostic potential of modified VCG in detecting functional and structural alterations, specifically with impaired systolic function and LVH. The study will assess whether VCG provides enhanced viability as a faster, more cost-effective, and accessible non-invasive diagnostic tool for clinical practice.

Methods

Study design

This prospective case-control study enrolled patients with impaired systolic function, patients with left ventricular hypertrophy (LVH), as well as patients presenting with both reduced LV-EF and LVH, in order to investigate specific patterns in VCG signals associated with cardiac dysfunctions and the degree of structural remodeling. The overall analytical workflow for identifying structural cardiac abnormalities using VCG is summarized in Fig. 1.

Setting

The study was conducted at the Department of Cardiology, Angiology, and Pneumology at Heidelberg University Hospital. Between January 2023 and February 2024, potential participants underwent cardiac magnetic resonance imaging (CMR) as part of routine clinical practice. These CMR examinations were performed to identify functional or structural heart disease based on clinical indications.

The recruitment and examinations were conducted in accordance with the guidelines of the Ethics Committee (S-421/2022) of the Medical Faculty of Heidelberg and the current version of the Declaration of Helsinki. All patients and controls received detailed information, and all procedures were carried out only after obtaining written informed consent.

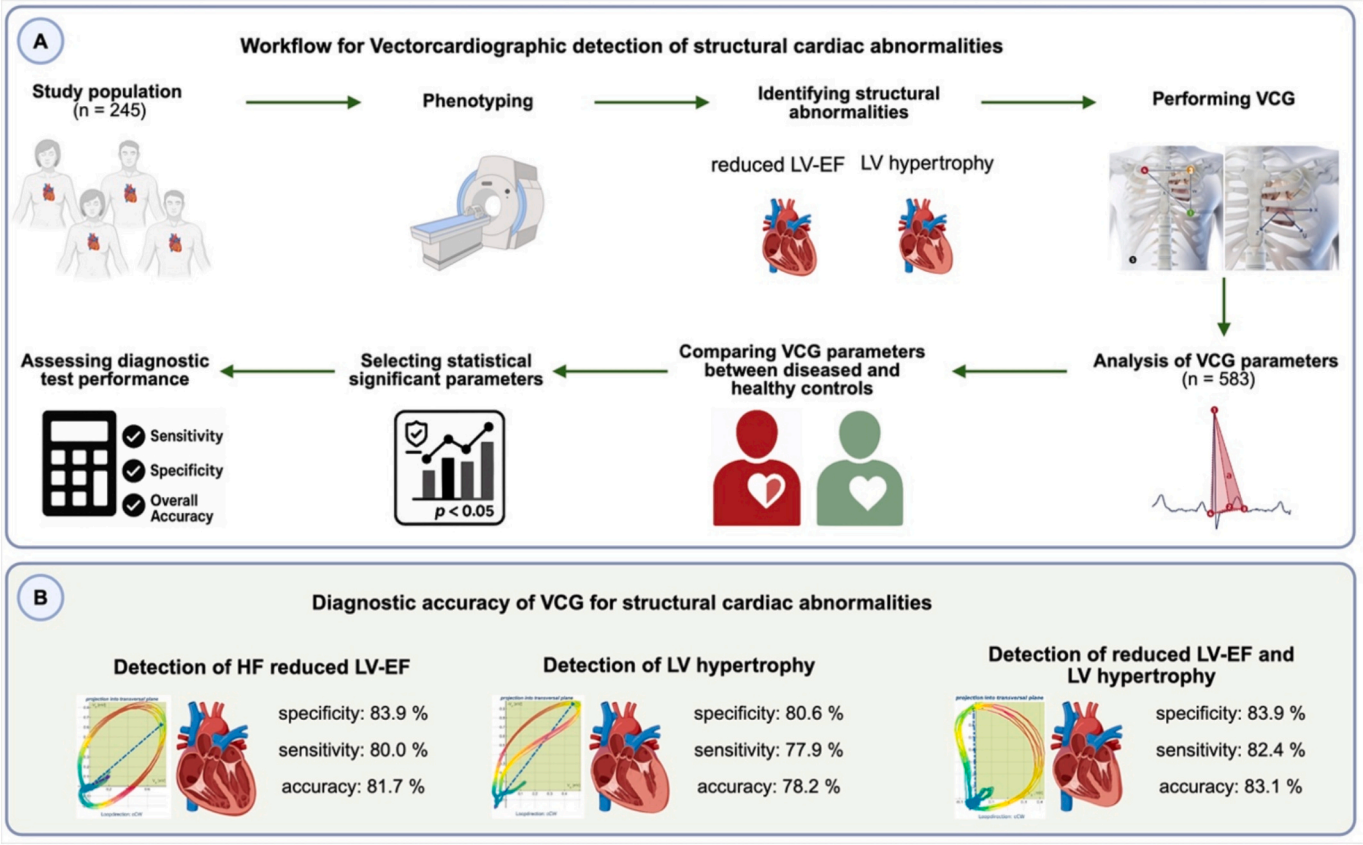

Fig. 1. (Graphical abstract) Vectorcardiographic assessment of structural cardiac abnormalities: workflow and diagnostic accuracy.
Footnote: Structural cardiac abnormalities were defined as reduced left ventricular ejection fraction (LV-EF), the presence of left ventricular hypertrophy (LVH), or the combination of both conditions. Vectorcardiographic (VCG) parameters were extracted from affected patients and healthy controls. Statistical testing identified parameters that significantly differentiated disease from control. Sensitivity, specificity, and overall diagnostic accuracy were calculated for each group. Panel A illustrates the analytical workflow, while Panel B summarizes diagnostic performance results for reduced LV-EF, LVH, and the combined phenotype.
VCG: vectorcardiography; EF: ejection fraction; LV: left ventricle.

Participants

Patients with reduced left ventricular ejection fraction (LV-EF) were classified as Group 1 (LVEF <40%). Patients with left ventricular hypertrophy (LVH, indexed LV mass $\geq$ 55 g/m^2) were classified as Group 2. Patients presenting both reduced LV-EF (<40%) and LVH were classified as Group 3 (overlap group).

Selection of controls

To enable a comparison of VCG parameters, subjects without functional or structural abnormalities were included as controls. The indication for CMR examination in the control group was based on clinical criteria aimed at ruling out structural anomalies or pathological changes. Control group data were evaluated in the same manner as those of the patient groups. Exclusion criteria for the control group included any previous cardiovascular events (e.g., myocardial infarction, coronary artery disease), the presence of infarct-related Late gadolinium enhancement (LGE), or conditions such as hypertensive heart disease, amyloidosis, Takotsubo cardiomyopathy, non-compaction cardiomyopathy, acute myocarditis, or congenital heart defects.

Vectorcardiographic signal acquisition

Vectorcardiographic signals were acquired using a five-electrode thoracic configuration (cardisiography; Cardisio GmbH, Frankfurt, Germany), a vectorcardiography-based recording technique that reconstructs three-dimensional cardiac electrical vectors from surface potentials. As previously described (12), three signal electrodes and one ground electrode were positioned in a predefined geometric arrangement on the anterior chest wall, while a fourth signal electrode was placed on the lower left side of the back to capture the third spatial dimension. From the resulting bipolar leads (H0, A, Ve, I, D), three-dimensional spatial vectors were computed using orthogonal projection into a Cartesian coordinate system (x, y, z), according to the transformation described by Sanz (15).

All recordings were performed at rest over a four-minute acquisition period. Fiducial points, including QRS onset and offset, R-peak, Tonset, and T-wave end, were determined automatically using the proprietary signal-processing pipeline implemented in the Cardisiography system. QRS detection was performed using wavelet-based analysis, which enables robust identification of localized depolarization landmarks despite varying signal characteristics. T-wave delineation, including Tonset, was based on previously described approaches calibrated by clinical knowledge (16), combined with further refinements developed by the Cardisiography research and clinical team. These methods incorporate both signal morphology and physiological constraints to improve the robustness of T-wave boundary detection. Cross-lead information from the full multi-lead VCG signal set was incorporated to improve temporal precision and robustness. All fiducial points were derived automatically as part of the standardized Cardisiography analysis pipeline without manual annotation. The general methodological principles are based on established signal-processing approaches and clinically guided waveform delineation. Intervals were therefore derived from the integrated multi-lead signal representation rather than from a single lead in isolation.

Discriminating parameters were calculated as a dimensionless repolarization time-difference ratio (e.g. (Rpeak–Tonset)/(QRSend–T-peak)). From the resulting VCG time series, 583 parameters were extracted using an AI-assisted signal-processing framework. These parameters comprised geometric, spatial, and temporal descriptors of depolarization and repolarization, including vector magnitude, angular orientation (e.g., azimuth), velocity, acceleration, dispersion metrics, and loop-based features.

From this multidimensional parameter space, a set of candidate features was extracted for subsequent statistical evaluation against CMR-derived reference standards.

Cardiac magnetic resonance imaging

Standard CMR was performed on 1.5 T or 3 T Philips Ingenia™ scanners (Philips Healthcare, Best, The Netherlands) with a phased array receiver coil (17). Standard cine long-axis (2-, 3-, and 4-chamber) and contiguous short-axis stacks covering the LV were acquired using breath-hold bSSFP sequences with retrospective ECG or pulse-oximetry gating. Typical parameters were TR 2.8–2.9 ms, TE 1.4 ms, flip angle 45–60°, 35–40 phases per cardiac cycle, and breath-hold time 7–10 s per slice. Volumetric analysis was performed with CVI42 (Circle Cardiovascular Imaging, Calgary, Canada) and vendor workstations (Viewforum™ and IntelliSpace™ Portal, ISP™, Philips Healthcare, Best, The Netherlands). LV and RV volumes, ejection fraction, and LV myocardial mass were derived from manual tracing of *endo*- and epicardial contours, excluding papillary muscles.

Late gadolinium enhancement

LGE imaging was performed 10 min after intravenous administration of gadobutol (Gadovist™, Bayer HealthCare, Leverkusen, Germany) using a T1-weighted inversion recovery gradient-echo sequence with individually optimized inversion time. Imaging was repeated in an orthogonal plane to confirm findings, according to established protocols (18).

Statistical analysis

Statistical analysis was performed using MedCalc™, version 23.0.2 (Ostend, Belgium) and MATLAB (version2020a) with $p < 0.05$ taken to indicate statistical significance for all statistical tests. Continuous variables were tested for normality using the Kolmogorov–Smirnov test. Normally distributed data are presented as mean ± standard deviation and were compared between groups using one-way analysis of variance (ANOVA), with post-hoc pairwise comparisons using the independent *t*-test where appropriate. Non-normally distributed variables are reported as median and interquartile range (IQR) and were compared using the Kruskal–Wallis test, followed by pairwise Mann–Whitney *U* tests where indicated. Categorical variables are expressed as counts and percentages and were compared using the chi-square test.

For diagnostic evaluation of individual VCG parameters, ROC curve analyses were performed using CMR-defined reduced LV-EF (<40%), LVH (indexed LV mass $\geq$ 55 g/m^2), or the combination of both as reference standards. The analytical framework was designed as a binary classification model (reduced vs. non-reduced LV-EF) based on the predefined CMR threshold; no regression model was fitted to predict continuous LV-EF values. Diagnostic performance was assessed by calculating the area under the ROC curve (AUC), as well as sensitivity, specificity, positive predictive value (PPV), negative predictive value (NPV), and overall accuracy at the optimal operating point.

For individual VCG parameters, optimal cut-off values were derived from receiver operating characteristic (ROC) curve analysis using the Youden index. These thresholds were determined on the basis of the full available dataset and were not derived from separate training and validation subsets. Various ECG and VCG parameters, as well as Frenet–Serret descriptors, were taken into consideration. The classification for Groups 1 and 3 is based on the individually selected single parameter. Classification performance is determined by selecting a suitable threshold from the ROC curve. The classification for Group 2 is based on three parameters, which are mapped via Bayes' theorem to the posterior probability of a patient being positive conditional on a given measurement. The Bayesian model is calibrated using data from 208 positive and 31 negative patients, while accounting, without loss of generality, for the corresponding prevalence. A patient is classified as positive if the posterior probability of positivity, after incorporating the three

measurement-specific parameters, exceeds the patient's prior probability of being positive; otherwise, the patient is classified as negative. Although the posterior probability depends on the assumed prevalence, the present classification rule labels a patient as positive whenever the posterior probability exceeds the prior probability. Hence, the binary classification rule is invariant to the specific choice of prevalence, whereas the numerical posterior probabilities remain prevalence dependent.

Model performance—specifically sensitivity, specificity, positive predictive value (PPV), negative predictive value (NPV), and overall accuracy— was calculated using a parameter threshold for groups 1 and 3. For group 2, classification was based on comparing the posterior probability from the Bayesian model (derived from the three selected parameters) with the prevalence, serving as the prior probability threshold. Accuracy was defined as (true positives + true negatives) / (true positives + true negatives + false positives + false negatives).

Results

Baseline characteristics of the study population

A total of 245 individuals were included in the study, comprising patients with structural and/or functional cardiac abnormalities as well as control subjects without detectable abnormalities on CMR. Groups were defined a priori based on CMR and were not mutually exclusive with respect to reduced LV-EF and LVH; specifically, group 3 represents the overlap of these two phenotypes. Among the 245 participants, 40 patients had reduced left ventricular ejection fraction (LV-EF < 40%) on cardiac MRI (group 1). 208 patients showed left ventricular hypertrophy (LVH) with an indexed LV mass of 67 g/m^2 (IQR 61–77 g/m^2; group 2). Of the 40 patients with reduced LVEF, 34 also fulfilled criteria for LVH (overlap, group 3), leaving 6 patients with isolated reduced LVEF. The control group (group 4) consisted of 31 individuals with normal cardiac structure and function (mean LV-EF 62 ± 5.6%, indexed LV mass 40 g/m^2 [IQR 35–47 g/m^2]).

Of the entire study population, 47 participants (16.8%) were female. Patients with LVH were predominantly male (86.5%) and significantly older than controls (63 vs. 54 years, $p < 0.001$). Individuals with combined LV dysfunction and hypertrophy (group 3) showed a similar age distribution to those with reduced LV-EF alone but tended to be slightly older than controls.

Left ventricular ejection fraction differed markedly between groups ($p < 0.0001$). Median LV-EF was 32% (IQR 23–37) in groups 1 and 3, 54% (IQR 45–63) in the LVH group, and 62% (IQR 57–66) in controls.

Regarding symptom classification, no significant group differences were observed for Canadian Cardiovascular Society (CCS) classification, while New York Heart Association (NYHA) class was significantly higher in patients with reduced LV-EF compared with controls ($p < 0.05$ for group 1 vs. 4; $p < 0.01$ for group 3 vs. 4), indicating more frequent exertional dyspnea in these groups.

Cardiovascular risk factors were common across all subgroups. Smoking was more frequent among patients with reduced LV-EF (group 1) (35.0%). Arterial hypertension was most prevalent in the LVH group (68.3%). Smoking differed significantly across groups, whereas the other cardiovascular risk factors did not show significant between-group differences. Detailed demographic, clinical, and imaging characteristics are summarized in Table 1.

Vectorcardiography in patients with reduced ejection fraction

Among the 583 vectorcardiographic (VCG) parameters analyzed, the repolarization time-difference ratio (Rpeak–Tonset / QRSend–Tpeak) showed the highest diagnostic utility for identifying patients with reduced left ventricular ejection fraction (LV-EF) (Table 2, **Supplementary Fig. S1**). This dimensionless ratio reflects the relative timing of repolarization landmarks within the cardiac cycle and does not involve the RR interval. When compared to cardiac magnetic resonance imaging (CMR) as the reference standard, the repolarization time-difference ratio

Table 1
Baseline characteristics, Values are mean ± standard deviation, median (interquartile range), or n (%).

Patient characteristics	Reduced LV-EF (n = 40) (group 1)	LV-hypertrophy (n = 208) (group 2)	Reduced LV-EF and LVH (n = 34) (group 3)	Control group (n = 31) (group 4)	Group comparison	1 vs. 2	1 vs. 4	2 vs. 4	3 vs. 4
Age (years)	57 (44–69)	63 (49–71)	59 (43–69)	54 (39–61)	<0.05	0.118	0.122	**<0.001**	0.107
Male, n (%)	31 (77.5)	180 (86.5)	27 (79.4)	21 (67.7)	<0.05	0.143	0.360	**<0.05**	0.289
BMI (kg/m^2)	27 (25–30)	27 (24–31)	27 (25–32)	25 (22–32)	0.537	–	–	–	
LV-EF (%)	32 (23–37)	54 (45–63)	32 (24–37)	62 (57–66)	**<0.0001**	**<0.0001**	**<0.0001**	**<0.0001**	**<0.0001**
CCS classification	0 (0–1)	0 (0–0.25)	0 (0–1)	0 (0–0.75)	0.941	–	–	–	
NYHA classification	1 (0–2)	0 (0–2)	0 (0–2)	0 (0–1)	**<0.05**	**<0.05**	**<0.01**	0.191	**<0.01**
Cardiovascular risk factors									
Smoking, n (%)	14 (35.0)	42 (20.2)	13 (38.2)	6 (19.4)	0.037	**<0.05**	–	–	
Arterial hypertension, n (%)	23 (57.5)	142 (68.3)	20 (58.8)	15 (48.4)	0.109	–	–	–	
Family history of CV-disease	19 (47.5)	94 (45.2)	14 (41.2)	14 (45.2)	0.959	–	–	–	
Diabetes mellitus, n (%)	5 (12.5)	22 (10.6)	5 (14.7)	1 (3.2)	0.467	–	–	–	
Hypercholesterolemia, n (%)	17 (42.5)	101 (48.6)	13 (38.2)	11 (35.5)	0.406	–	–	–	

Footnote: Baseline characteristics of the study population across four groups: patients with reduced LV-EF, patients with LV hypertrophy, patients with both reduced LV-EF and LVH, and controls. This includes demographic data, cardiac function, and cardiovascular risk factors across three groups: patients with reduced LV-EF, patients with LV hypertrophy, and controls. Continuous variables are presented as median (25th–75th percentile). Group comparisons for non-normally distributed variables were performed using the Kruskal–Wallis test. Categorical variables were compared using the Chi-square test.
CCS = Canadian Cardiovascular Society classification (I–IV); NYHA = New York Heart Association classification (I–IV); LV = left ventricle; EF = ejection fraction; BMI = body mass index.

Table 2
Discriminative vectorcardiographic parameters in patients with reduced left-ventricular ejection fraction or left-ventricular hypertrophy vs. controls.

Parameters	Repolarization time-difference ratio (1)	T-wave azimuth (2)	T-wave magnitude (3)	Azimuth variability (4)	Repolarization time-difference ratio (5)
Used for discrimination	Reduced LV-EF	LVH	LVH	LVH	Reduced LV-EF + LVH
Unit		Azimuth (rad)	Magnitude (mV)	Azimuth (rad)	
AUC	84.3%	79.0%	79.1%	73.9%	86.6%
P-value (adjusted)	5.01E-04	1.14E-04	1.08E-04	1.02E-02	2.40E-04
Patients (n)	40	208	208	208	34
Control group (n)	31	31	31	31	31
Patients mean + SD	1.14 ± 0.26	0.69 ± 0.24	0.32 ± 0.89	0.11 ± 0.17	1.12 ± 0.23
Control mean + SD	1.41 ± 0.15	0.46 ± 0.22	0.08 ± 0.03	0.19 ± 0.13	1.41 ± 0.15
Patients Skewness	0.19	−1.17	5.27	2.52	−0.29
Control Skewness	0.11	−0.22	1.09	0.72	0.11
Patients Kurtosis	3.59	4.20	33.06	9.78	3.05
Control Kurtosis	2.79	1.88	5.84	3.21	2.79

Footnote: Values are presented for selected VCG parameters with the highest diagnostic performance in distinguishing patients from control subjects. **Mean ± SD** indicates the average value and its dispersion within each group. **Skewness** reflects the asymmetry of the data distribution (positive = right-skewed; negative = left-skewed). **Kurtosis** describes the peakedness or heaviness of the distribution tails (higher values indicate sharper peaks or more outliers). (**1**) and (**5**) Repolarization time-difference ratio (Rpeak–Tonset / QRSend–Tpeak). (**2**) T-wave azimuth: Curvature of the T-wave loop vector in the horizontal plane. (**3**) T-wave magnitude: Median electrical amplitude of the T-wave. (**4**) Azimuth variability: Temporal variability of the T-wave azimuth over time.
AUC = area under the curve; mV = millivolt; rad = radians; SD = standard deviation; Bonferroni adjustment for *P*-value.

achieved a sensitivity of 80.0%, a specificity of 83.9%, a positive predictive value (PPV) of 86.5%, and a negative predictive value (NPV) of 76.5%, resulting in an overall diagnostic accuracy of 81.7% (Table 3, Fig. 2).

Vectorcardiography in patients with left ventricular hypertrophy

In patients with LVH, three VCG parameters demonstrated relevant diagnostic performance: T-wave azimuth, T-wave magnitude, and azimuth variability (Table 2, **Supplementary Fig. S2**). The T-wave azimuth quantifies the angular position of the T-wave loop vector in the horizontal plane and reflects directional changes in ventricular repolarization over time. T-wave magnitude, expressed in millivolts, represents the median amplitude of the repolarization vector. Azimuth variability reflects temporal fluctuations in the horizontal direction of the electrical vector.

Compared with CMR-defined LVH, the combination of these three parameters yielded a sensitivity of 77.9%, specificity of 80.6%, PPV of 96.4%, and NPV of 35.2%, corresponding to an overall diagnostic accuracy of 78.2% (Table 3, Fig. 2).

Table 3
Evaluation of diagnostic metrics for Vectorcardiography-based detection of reduced left ventricular ejection fraction and left ventricular hypertrophy.

Diagnostic performance metrics	Reduced LV-EF (group 1)	LVH (group 2)	Reduced LV-EF and LVH (group 3)
Sensitivity	80.0%	77.9%	82.4%
Specificity	83.9%	80.6%	83.9%
Positive predictive value (PPV)	86.5%	96.4%	84.8%
Negative predictive value (NPV)	76.5%	35.2%	81.3%
Accuracy	81.7%	78.2%	83.1%

Footnote: Diagnostic performance of the most discriminative vectorcardiographic (VCG) parameters in identifying patients with reduced left ventricular ejection fraction (LV-EF), left ventricular hypertrophy (LVH), or both conditions combined (EF & LVH), using CMR as the reference standard. Parameters used for discrimination: **repolarization time-difference ratio (Rpeak–Tonset / QRSend–Tpeak)** for reduced LV-EF and for the combined phenotype (reduced LV-EF + LVH); **T-wave azimuth, T-wave magnitude, and azimuth variability** for LVH.
EF = ejection fraction; LV = left ventricle; VCG = vectorcardiography.

Vectorcardiography in patients with concomitant reduced ejection fraction and left ventricular hypertrophy

In patients presenting with both reduced LV-EF and LVH, the repolarization time-difference ratio again emerged as the most discriminative parameter compared with controls. It achieved an AUC of 86.6% (Table 2, **Supplementary Fig. S3**). At the optimal operating point, diagnostic performance was: sensitivity 82.4%, specificity 83.9%, PPV 84.8%, NPV 81.3%, and overall accuracy 83.1% (Table 3). Representative cardiac vector loops and ROC curves illustrating the most discriminative VCG parameters across groups 1, 2, and 3 are shown in Fig. 2.

Discussion

Summary of main findings

This study assessed the diagnostic value of VCG for detecting left ventricular systolic dysfunction and hypertrophy, using CMR as the reference standard. Among the 583 VCG-derived parameters analyzed, selected markers showed high diagnostic accuracy in distinguishing patients with reduced ejection fraction and those with left ventricular hypertrophy from controls. The VCG approach demonstrated good sensitivity and specificity, supporting its potential as a non-invasive and accessible tool for early detection of structural and functional cardiac abnormalities.

Physiological interpretation of selected VCG features

The most informative VCG parameter for detecting reduced LVEF was a repolarization time-difference ratio (Rpeak–Tonset / QRSend–Tpeak), reflecting the relative timing of repolarization landmarks within the cardiac cycle. A prolonged QT interval in relation to the cardiac cycle may indicate delayed ventricular repolarization and has been associated with an increased risk of arrhythmias (19).

In patients with LVH, three VCG-derived features contributed most to diagnostic performance: the T-wave azimuth, the T-wave magnitude, and azimuth variability. The T-wave azimuth quantifies the curvature of the repolarization vector in the horizontal plane, capturing directional changes in ventricular repolarization over time. Similar findings were reported by Bury et al., who showed that the azimuth of the spatial ventricular gradient significantly differed between patients with and without cardiac events in long QT syndrome, supporting its role as a

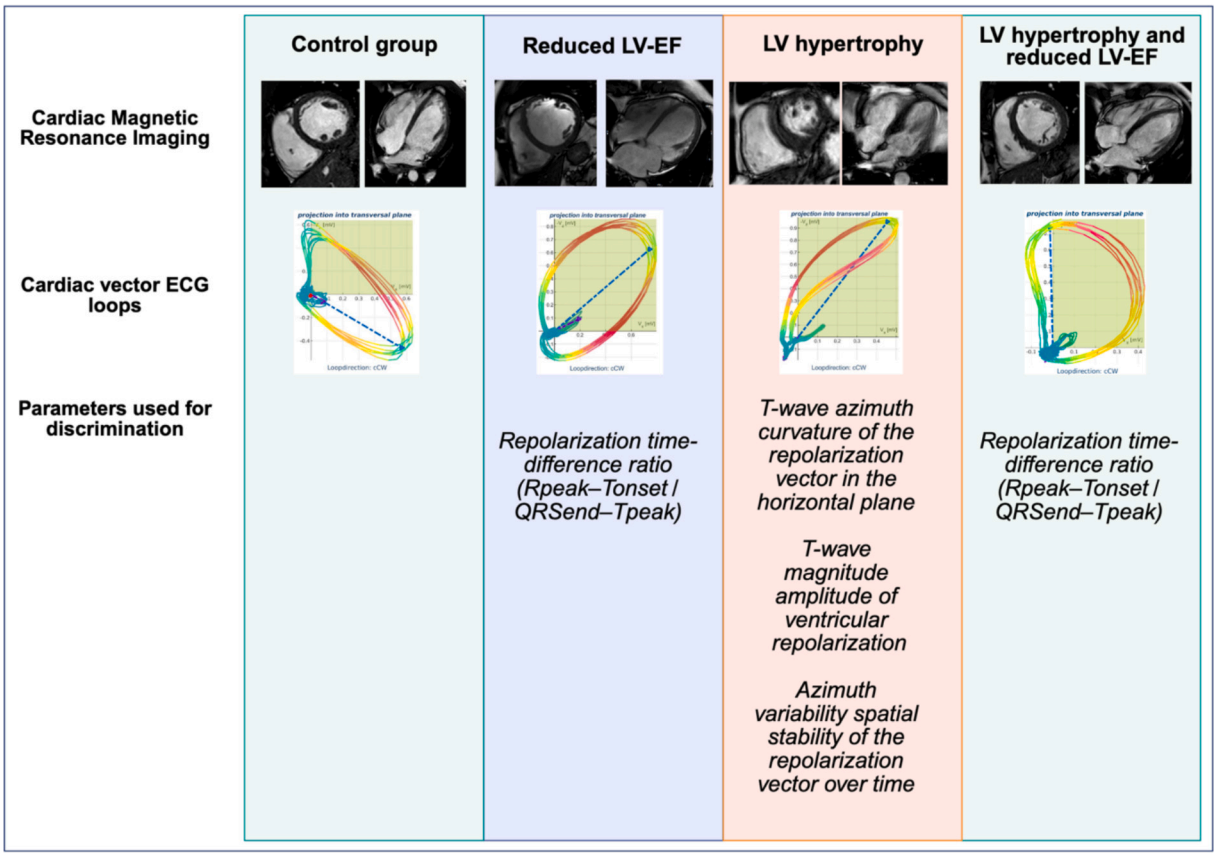

Fig. 2. Diagnostic discrimination of structural cardiac abnormalities using vectorcardiographic features.
Footnote: Cardiac vector loops and ROC curve analyses illustrate the ability of vectorcardiography (VCG) to discriminate between controls and individuals with reduced LV-EF, LV hypertrophy, or both conditions combined.
Diagnostic performance is shown for key repolarization parameters, including repolarization time-difference ratio (Rpeak–Tonset / QRSend–Tpeak), T-wave azimuth, T-wave magnitude, and azimuth variability.
AUC: area under the curve; VCG: vectorcardiography; LV-EF: left ventricular ejection fraction; LV: left ventricle.

marker of repolarization heterogeneity and electrical instability (20). Increased curvature in azimuth may reflect non-linear, heterogeneous repolarization patterns commonly seen in structural remodeling.

T-wave magnitude represents the overall amplitude of ventricular repolarization. Its diagnostic value is supported by data from magnetocardiographic studies, where beat-to-beat variability in T-wave amplitude demonstrated strong discriminatory power for detecting ischemic heart disease (21). Moreover, a study by Jimenez et al. showed that reduced T-wave vector magnitude was associated with adverse cardiac events in pediatric patients with hypertrophic cardiomyopathy, emphasizing its prognostic relevance in the context of repolarization abnormalities (22). These findings reinforce the inclusion of T-wave magnitude as a meaningful parameter for detecting structural remodeling, such as LVH.

Azimuth variability estimates the spatial stability of the repolarization vector over time. Increased variability reflects a loss of directional coherence in ventricular repolarization and is indicative of repolarization heterogeneity. Prior studies have shown that transient increases in azimuth variability occur following changes in ventricular activation—such as after ablation of accessory pathways—and are associated with cardiac memory and spatial repolarization gradients (23). In our study, elevated azimuth variability was associated with LVH, suggesting greater directional dispersion of repolarization in structurally remodeled myocardium. This observation aligns with findings by Loring et al., who demonstrated that the azimuth orientation of the QRS loop shows considerable interindividual variability, partly influenced by anatomical factors such as papillary muscle positioning (24). These results highlight the complex interaction between structural remodeling and repolarization dynamics, as captured by VCG.

Comparison with existing literature

ECG remains a widely accessible and non-invasive diagnostic modality. However, its traditional role in detecting structural heart disease is limited by modest sensitivity. Recent advancements in AI have enhanced ECG's diagnostic capacity, particularly for identifying reduced LV-EF. In a rural high-risk population, Devkota et al. successfully predicted low ejection fraction using AI-based ECG, with key contributions from leads I, aVR, V2, and V3 (25). These findings are corroborated by a recent meta-analysis by Ferreira et al., which pooled results from over 145,000 patients and showed that AI-enhanced ECGs achieve high diagnostic accuracy for identifying LVEF <40%—with a pooled sensitivity of 84%, specificity of 80%, and an AUC of 0.917 (26). These results underscore the evolving role of AI-enhanced ECG as a scalable, cost-effective screening tool for early detection of cardiac dysfunction, with applications extending to primary care and resource-limited settings.

In contrast to these AI-ECG approaches, our study focuses on VCG as a diagnostic modality. Recently, Passow and Tenderich proposed a closed mathematical model describing the electric potential of the human myocardium throughout the QT interval, providing a theoretical framework for next-generation AI-enabled diagnostic methods such as Cardisiography (27). Rather than using standard 2D ECG waveforms, VCG captures the heart's electrical activity in three orthogonal spatial planes, enabling a more nuanced analysis of spatial and temporal vector dynamics. While most AI-ECG studies analyze entire waveforms through deep learning models, often with limited interpretability, our approach

systematically evaluates specific, physiologically interpretable VCG parameters. This not only allows for robust discrimination between patients with and without structural dysfunction but also yields insights into the underlying pathophysiological changes.

Recent studies have further validated the utility of VCG-based techniques. In a UK-based prospective community cohort, CSG—an AI-assisted VCG tool—proved feasible for use in primary care and pharmacy settings, demonstrating strong diagnostic performance and high patient acceptability (28). Similarly, Braun et al. confirmed the diagnostic value of CSG for detecting asymptomatic CAD, reporting diagnostic accuracies of 90.7% for men and 82.5% for women (12). These findings emphasize the growing potential of VCG, especially when enhanced by AI, as a rapid, non-invasive, and cost-effective screening modality for early cardiac dysfunction.

Clinical implications

Our findings suggest that VCG, may serve as a practical, time- and cost-effective diagnostic tool for identifying patients with reduced left ventricular ejection fraction and left ventricular hypertrophy. Unlike traditional imaging modalities such as echocardiography or CMR, VCG requires minimal operator expertise, no radiation, and can be conducted rapidly in outpatient or primary care settings. This makes it especially valuable in settings where access to advanced imaging is limited by cost, logistics, or availability.

Limitations

Several limitations of this study should be considered. First, this was a single-center, non-matched case-control study with a relatively small sample size and an imbalanced sex distribution, with only 16.8% female participants. The predominance of male participants likely reflects referral patterns for CMR in patients with suspected structural heart disease. This may limit the generalizability of our findings to broader, more diverse populations. Future research should aim to validate these results in larger, multi-center cohorts that include a more balanced representation of sex, age, and comorbidities.

Second, although 40 patients had reduced LVEF, only 6 presented with isolated systolic dysfunction without concomitant LVH. The limited size of this subgroup restricts the robustness of conclusions regarding isolated reduced LVEF. Accordingly, primary analyses were conducted for reduced LVEF overall and for the combined phenotype (reduced LVEF + LVH). Subgroup-specific findings should therefore be interpreted with caution and require validation in larger, independent cohorts.

Third, the study did not stratify patients according to the underlying etiology of reduced LV-EF or LVH. Etiological differences—such as ischemic versus non-ischemic cardiomyopathy—may influence VCG signal patterns and diagnostic performance. Future analyses should investigate whether specific VCG features can differentiate among etiologic subtypes, which could enhance the clinical utility of the method.

Fourth, while individuals in the control group had normal findings on cardiac MRI, the presence of subclinical cardiovascular disease—particularly coronary artery disease not evident on stress testing—cannot be fully excluded. However, this approach mirrors real-world clinical settings, where diagnostic uncertainty often persists despite advanced imaging.

In addition, although artificial intelligence was used to assist in VCG signal interpretation, the employed algorithm has not yet been externally validated in independent populations. Thresholds for individual VCG parameters were derived within the study cohort and were not externally validated. Therefore, these cut-off values should be considered exploratory and hypothesis-generating. Limitations of AI include risks of overfitting, dependence on high-quality input data, and restricted generalizability across different clinical settings. Further development and prospective validation of these AI models in larger, heterogeneous datasets are required.

Lastly, the acceptability and widespread implementation of VCG as a diagnostic tool will depend on considerations related to infrastructure requirements, and integration into existing clinical workflows. Addressing these factors is essential for clinical translation.

The present study focused on classification rather than continuous LVEF estimation. Future research should assess whether regression-based VCG models can accurately predict absolute LVEF values.

Conclusion

This study highlights the diagnostic potential of VCG as a non-invasive tool for identifying patients with reduced LV-EF and LVH. Importantly, our findings support the use of VCG as a scalable screening tool for early identification of subclinical cardiac disease. Its rapid acquisition, minimal operator dependency, and low cost make it particularly well-suited for use in community-based settings, primary care, and regions with limited access to advanced imaging modalities.

If validated in larger, diverse populations, VCG—combined with AI-based analysis—could fill an important gap in cardiovascular screening strategies, enabling earlier intervention, better risk stratification, and potentially improved long-term outcomes.

Ethics approval and informed consent

The study was approved by the Ethics Committee of the Medical Faculty of Heidelberg (S-421/2022) and was conducted in accordance with the Declaration of Helsinki. Written informed consent was obtained from all study participants.

CRediT authorship contribution statement

Janek Salatzki: Writing – review & editing, Writing – original draft, Visualization, Supervision, Project administration, Methodology, Investigation, Formal analysis, Data curation, Conceptualization. **Arne Kristian Schwarz:** Writing – review & editing, Writing – original draft, Visualization, Validation, Supervision, Software, Resources, Methodology, Investigation, Formal analysis, Data curation, Conceptualization. **Sarah Wolfsteller:** Writing – review & editing, Software, Methodology, Formal analysis, Data curation. **Nicolas Hein:** Writing – review & editing, Writing – original draft, Visualization, Methodology, Investigation, Formal analysis. **Erika Poyo Medina:** Writing – review & editing, Software, Formal analysis, Data curation. **Norbert Frey:** Writing – original draft, Validation, Resources, Funding acquisition. **Henning Steen:** Writing – review & editing, Supervision, Funding acquisition, Conceptualization. **Florian André:** Writing – review & editing, Resources, Funding acquisition, Conceptualization. **Alexander Passow:** Writing – review & editing, Writing – original draft, Validation, Supervision, Software, Resources, Project administration, Methodology, Investigation, Formal analysis, Conceptualization.

Declaration of competing interest

Janek Salatzki received research funding from the German Centre for Cardiovascular Research (DZHK), the German Heart Foundation, and from Cardisio GmbH. Arne Kristian Schwarz and Alexander Passow report employment or consultancy with Cardisio GmbH.

Acknowledgement

We thank our technologists at the Department of Cardiology, Angiology and Pneumology at Heidelberg University Hospital for image acquisition.

Appendix A. Supplementary data

Supplementary data to this article can be found online at https://doi.org/10.1016/j.jelectrocard.2026.154272.

References

[1] Virani SS, Alonso A, Aparicio HJ, Benjamin EJ, Bittencourt MS, Callaway CW, et al. Heart disease and stroke Statistics-2021 update: a report from the American Heart Association. Circulation 2021;143(8):e254–743. https://doi.org/10.1161/CIR.0000000000000950 [PubMed PMID: 33501848].

[2] Shahim B, Kapelios CJ, Savarese G, Lund LH. Global public health burden of heart failure: an updated review. Card Fail Rev 2023;9:e11. https://doi.org/10.15420/cfr.2023.05. PubMed PMID: 37547123; PubMed Central PMCID: PMC10398425.

[3] Verdecchia P, Carini G, Circo A, Dovellini E, Giovannini E, Lombardo M, et al. Left ventricular mass and cardiovascular morbidity in essential hypertension: the MAVI study. J Am Coll Cardiol 2001;38(7):1829–35. https://doi.org/10.1016/s0735-1097(01)01663-1 [PubMed PMID: 11738281].

[4] Haider AW, Larson MG, Benjamin EJ, Levy D. Increased left ventricular mass and hypertrophy are associated with increased risk for sudden death. J Am Coll Cardiol 1998;32(5):1454–9. https://doi.org/10.1016/s0735-1097(98)00407-0 [PubMed PMID: 9809962].

[5] Docherty KF, Lam CSP, Rakisheva A, Coats AJS, Greenhalgh T, Metra M, et al. Heart failure diagnosis in the general community - who, how and when? A clinical consensus statement of the Heart Failure Association (HFA) of the European Society of Cardiology (ESC). Eur J Heart Fail 2023;25(8):1185–98. https://doi.org/10.1002/ejhf.2946 [PubMed PMID: 37368511].

[6] McDonagh TA, Metra M, Adamo M, Gardner RS, Baumbach A, Böhm M, et al. 2021 ESC guidelines for the diagnosis and treatment of acute and chronic heart failure: developed by the Task Force for the diagnosis and treatment of acute and chronic heart failure of the European Society of Cardiology (ESC). With the special contribution of the Heart Failure Association (HFA) of the ESC. Eur J Heart Fail 2022;24(1):4–131. https://doi.org/10.1002/ejhf.2333. PubMed PMID: 35083827.

[7] Arbelo E, Protonotarios A, Gimeno JR, Arbustini E, Barriales-Villa R, Basso C, et al. 2023 ESC guidelines for the management of cardiomyopathies. Eur Heart J 2023;44(37):3503–626. https://doi.org/10.1093/eurheartj/ehad194 [PubMed PMID: 37622657].

[8] Khan NK, Goode KM, Cleland JGF, Rigby AS, Freemantle N, Eastaugh J, et al. Prevalence of ECG abnormalities in an international survey of patients with suspected or confirmed heart failure at death or discharge. Eur J Heart Fail 2007;9(5):491–501. https://doi.org/10.1016/j.ejheart.2006.11.003 [PubMed PMID: 17218150].

[9] Bacharova L, Estes EH. Left ventricular hypertrophy by the surface ECG. J Electrocardiol 2017;50(6):906–8. https://doi.org/10.1016/j.jelectrocard.2017.06.006 [PubMed PMID: 28651797].

[10] Frank E. An accurate, clinically practical system for spatial vectorcardiography. Circulation 1956;13(5):737–49. https://doi.org/10.1161/01.cir.13.5.737 [PubMed PMID: 13356432].

[11] Vondrak J, Penhaker M. Review of processing pathological vectorcardiographic records for the detection of heart disease. Front Physiol 2022;13:856590. https://doi.org/10.3389/fphys.2022.856590. PubMed PMID: 36213240; PubMed Central PMCID: PMC9536877.

[12] Braun T, Spiliopoulos S, Veltman C, Hergesell V, Passow A, Tenderich G, et al. Detection of myocardial ischemia due to clinically asymptomatic coronary artery stenosis at rest using supervised artificial intelligence-enabled vectorcardiography - a five-fold cross validation of accuracy. J Electrocardiol 2020;59:100–5. https://doi.org/10.1016/j.jelectrocard.2019.12.018 [PubMed PMID: 32036110].

[13] Kardys I, Kors JA, van der Meer IM, Hofman A, van der Kuip DAM, Witteman JCM. Spatial QRS-T angle predicts cardiac death in a general population. Eur Heart J 2003;24(14):1357–64. https://doi.org/10.1016/s0195-668x(03)00203-3 [PubMed PMID: 12871693].

[14] Oehler A, Feldman T, Henrikson CA, Tereshchenko LG. QRS-T angle: a review. Ann Noninvasive Electrocardiol 2014;19(6):534–42. https://doi.org/10.1111/anec.12206. PubMed PMID: 25201032; PubMed Central PMCID: PMC4237708.

[15] Sanz E, Steger JP, Thie W. Cardiogoniometry. Clin Cardiol 1983;6(5):199–206. https://doi.org/10.1002/clc.4960060502 [PubMed PMID: 6851278].

[16] Elgendi M, Eskofier B, Abbott D. Fast T wave detection calibrated by clinical knowledge with annotation of P and T waves. Sensors 2015;15(7):17693–714. https://doi.org/10.3390/s150717693. PubMed PMID: 26197321; PubMed Central PMCID: PMC4541954.

[17] Salatzki J, Fischer T, Riffel J, André F, Hirschberg K, Ochs A, et al. Presence of contractile impairment appears crucial for structural remodeling in idiopathic left bundle-branch block. J Cardiovasc Magn Reson 2021;23(1):39. https://doi.org/10.1186/s12968-021-00731-6. PubMed PMID: 33789682; PubMed Central PMCID: PMC8015193.

[18] Schulz-Menger J, Bluemke DA, Bremerich J, Flamm SD, Fogel MA, Friedrich MG, et al. Standardized image interpretation and post processing in cardiovascular magnetic resonance: Society for Cardiovascular Magnetic Resonance (SCMR) board of trustees task force on standardized post processing. J Cardiovasc Magn Reson 2013;15(1):35. https://doi.org/10.1186/1532-429X-15-35. PubMed PMID: 23634753; PubMed Central PMCID: PMC3695769.

[19] Atiga WL, Calkins H, Lawrence JH, Tomaselli GF, Smith JM, Berger RD. Beat-to-beat repolarization lability identifies patients at risk for sudden cardiac death. J Cardiovasc Electrophysiol 1998;9(9):899–908. https://doi.org/10.1111/j.1540-8167.1998.tb00130.x [PubMed PMID: 9786070].

[20] Bury A, Day K, Cortez D. Decreased vector magnitudes may help identify events in patients with long QT syndrome. J Electrocardiol 2023;80:51–5. https://doi.org/10.1016/j.jelectrocard.2023.04.008 [PubMed PMID: 37196379].

[21] Senthilnathan S, Shenbaga Devi S, Sasikala M, Satheesh S, Selvaraj RJ. The role of beat-by-beat cardiac features in machine learning classification of ischemic heart disease (IHD) in magnetocardiogram (MCG). Biomed Phys Eng Express 2024;10(4). https://doi.org/10.1088/2057-1976/ad40b1 [PubMed PMID: 38640907].

[22] Jimenez E, El-Bokl A, Cortez D. Vectorcardiography as a prognostic tool in hypertrophic cardiomyopathy. J Electrocardiol 2021;68:80–4. https://doi.org/10.1016/j.jelectrocard.2021.08.004 [PubMed PMID: 34392139].

[23] Wecke L, Poçi D, Schwieler J, Johansson B, Edvardsson N, Lundahl G, et al. Vectorcardiography shows cardiac memory and repolarization heterogeneity after ablation of accessory pathways not apparent on ECG. Int J Cardiol 2013;166(1):152–7. https://doi.org/10.1016/j.ijcard.2011.10.106 [PubMed PMID: 22078977].

[24] Loring Z, Olson CW, Maynard C, Hakacova N. Modeling vectorcardiograms based on left ventricle papillary muscle position. J Electrocardiol 2011;44(5):584–9. https://doi.org/10.1016/j.jelectrocard.2011.06.010. PubMed PMID: 21872004; PubMed Central PMCID: PMC3169198.

[25] Devkota A, Prajapati R, El-Wakeel A, Adjeroh D, Patel B, Gyawali P. AI analysis for ejection fraction estimation from 12-lead ECG. Sci Rep 2025;15(1):13502. https://doi.org/10.1038/s41598-025-97113-0. PubMed PMID: 40251349; PubMed Central PMCID: PMC12008426.

[26] Ferreira ALC, Feitoza LPG de C, Benitez ME, Aziri B, Begic E, de Souza LVF, et al. Diagnostic accuracy of artificial-intelligence-based electrocardiogram algorithm to estimate heart failure with reduced ejection fraction: A systematic review and meta-analysis. Curr Probl Cardiol. 2025;50(4). https://doi.org/10.1016/j.cpcardiol.2025.103004. 103004, https://doi.org/10.1016/j.cpcardiol.2025.103004. PubMed PMID: 39909205.

[27] Passow A, Tenderich G. A mathematical approach to demonstrate R to T wave concordance of the human ECG. Sci Rep 2025;15(1):35759. https://doi.org/10.1038/s41598-025-20754-8. PubMed PMID: 41087510; PubMed Central PMCID: PMC12521502.

[28] Rudland SV, Shah NH, Nevill A. Community-based cardiovascular risk assessment using the cardisio(TM) AI test: a prospective cohort study. BJGP Open 2025: BJGPO.2024.0183. https://doi.org/10.3399/BJGPO.2024.0183 [PubMed PMID: 40389278].